Обзор ArXiv/astro-ph, 3-9 мая 2023 года

От Сильченко О.К.

ArXiv: 2305.04382

KURVS: The outer rotation curve shapes and dark matter fractions of $z \sim 1.5$ star-forming galaxies.

Annagrazia Puglisi[1,2]★, Ugnė Dudzevičiūtė[3], Mark Swinbank[1], Steven Gillman[4,5], Alfred L. Tiley[1,6], Richard G. Bower[1,7,8] Michele Cirasuolo[9], Luca Cortese[6,10], Karl Glazebrook[11], Chris Harrison[12], Edo Ibar[13], Juan Molina[14], Danail Obreschkow[6,15], Kyle A. Oman[7,16], Matthieu Schaller[17,18], Francesco Shankar[2], and Ray M. Sharples[19]

[1] *Centre for Extragalactic Astronomy, Department of Physics, Durham University, South Road, Durham DH1 3LE, UK*
[2] *School of Physics and Astronomy, University of Southampton, Highfield SO17 1BJ, UK*
[3] *Max-Planck-Institut für Astronomie, Königstuhl 17, D-69117, Heidelberg, Germany*
[4] *Cosmic Dawn Center (DAWN)*
[5] *DTU-Space, Technical University of Denmark, Elektrovej 327, DK-2800 Kgs. Lyngby, Denmark*
[6] *International Centre for Radio Astronomy Research, University of Western Australia, 35 Stirling Highway, Crawley, WA 6009, Australia*
[7] *Institute for Computational Cosmology, Durham University, South Road, Durham DH1 3LE, United Kingdom*
[8] *Institute for Data Science, Department of Physics, Durham University, South Road, Durham DH1 3LE, United Kingdom*
[9] *European Southern Observatory, Karl-Schwarzschild-Str 2, D-86748 Garching b. München, Germany*
[10] *ARC Centre of Excellence for All Sky Astrophysics in 3 Dimensions (ASTRO 3D), Australia*
[11] *Centre for Astrophysics and Supercomputing, Swinburne University of Technology, PO Box 218, Hawthorn, VIC 3122, Australia*
[12] *School of Mathematics, Statistics and Physics, Newcastle University, Newcastle upon Tyne NE1 7RU, UK*
[13] *Instiuto de Física y Astronomía, Universidad de Valparaíso, Avda. Gran Bretaña 1111, Valparaíso, Chile*
[14] *Department of Space, Earth and Environment, Chalmers University of Technology, Onsala Space Observatory, 439 92 Onsala, Sweden*
[15] *Australian Research Council Centre of Excellence for All-Sky Astrophysics, 44 Rosehill Street Redfern, NSW 2016, Australia*
[16] *Department of Physics, Durham University, South Road, Durham DH1 3LE, United Kingdom*
[17] *Lorentz Institute for Theoretical Physics, Leiden University, PO Box 9506, NL-2300 RA Leiden, The Netherlands*
[18] *Leiden Observatory, Leiden University, PO Box 9513, NL-2300 RA Leiden, The Netherlands*
[19] *Centre for Advanced Instrumentation, Department of Physics, Durham University, South Road, Durham DH1 3LE UK*

Глубокие наблюдения с KMOS

- В глубоком поле Chandra:
- 22 галактики
- Среднее красное смещение 1.5
- Средняя экспозиция 70 часов
- Средняя звездная масса (log) 10.2
- Средний эфф. радиус 3.7 кпк
- Пространственное разрешение (FWHM) 0.57”

Выборка

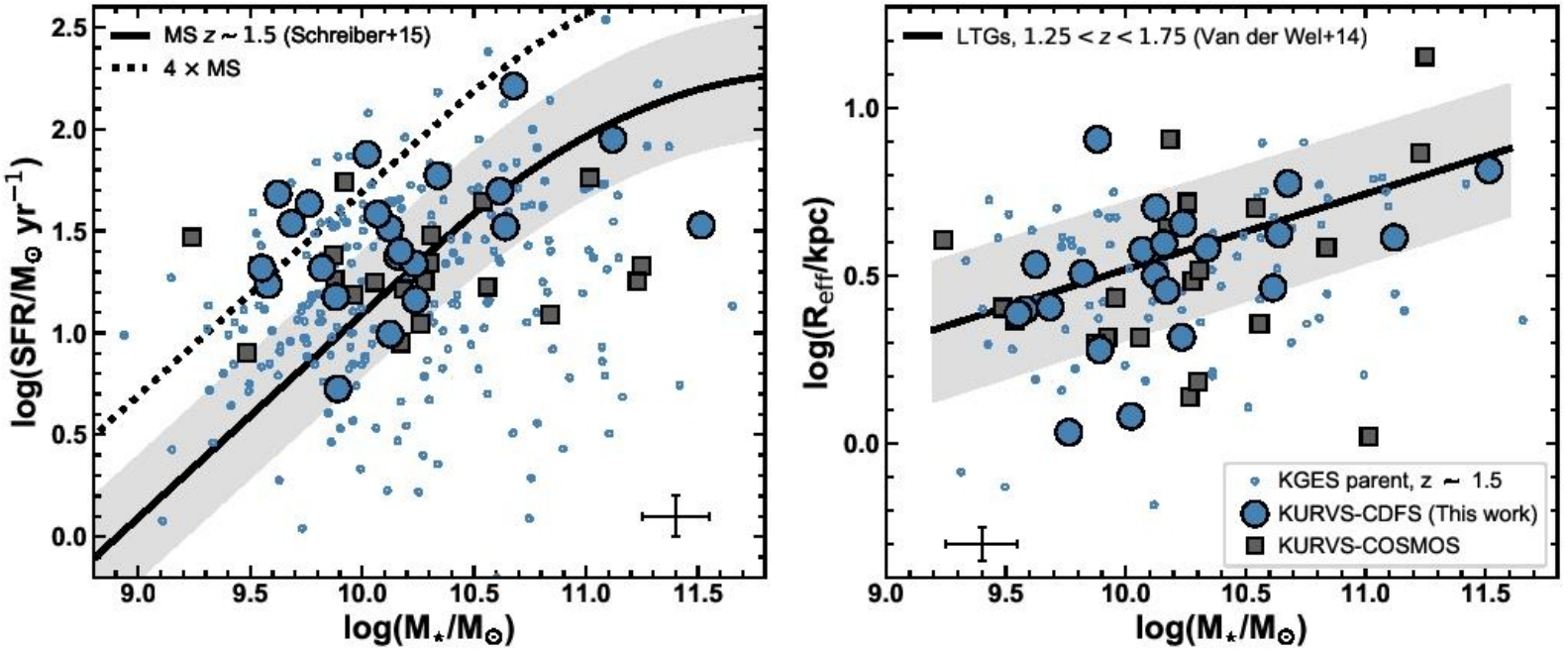

Figure 1. Left: Star formation rate as a function of stellar mass for our sample. Here the star formation rate of each galaxy is normalised to the SFR of the main sequence at $z \sim 1.5$, to account for the redshift evolution of the main sequence normalisation (e.g., Sargent et al. 2012). The blue filled circles correspond to KURVS galaxies in the CDFS field discussed in this work. Grey filled squares indicate KURVS galaxies in COSMOS, which will be presented in a forthcoming paper. Blue hollow circles show the parent sample from the KGES survey (Tiley et al. 2021). The median error bar for the KURVS and KGES points is shown in the bottom right. The solid line and shaded area indicate the position of the main sequence and its ±0.3 dex scatter from Schreiber et al. (2015) at $z = 1.5$, corresponding to the average redshift of the KURVS sample. The dashed line represents the factor of four threshold above which galaxies are usually classified as "starbursts". **Right:** Stellar half-light radius as a function of stellar mass for the KURVS sample. The median error bar for KURVS and KGES galaxies is shown in the bottom left. The black line and shaded area indicate the mass-size relation and its scatter at $1.25 < z < 1.75$ from Van der Wel et al. (2014). KURVS galaxies are located within the main-sequence and mass-size relations at the same redshift. Therefore, their star formation rate and structural properties suggest that KURVS galaxies represent typical star-forming systems at $z \sim 1.5$.

Пример глубокой панорамной спектроскопии

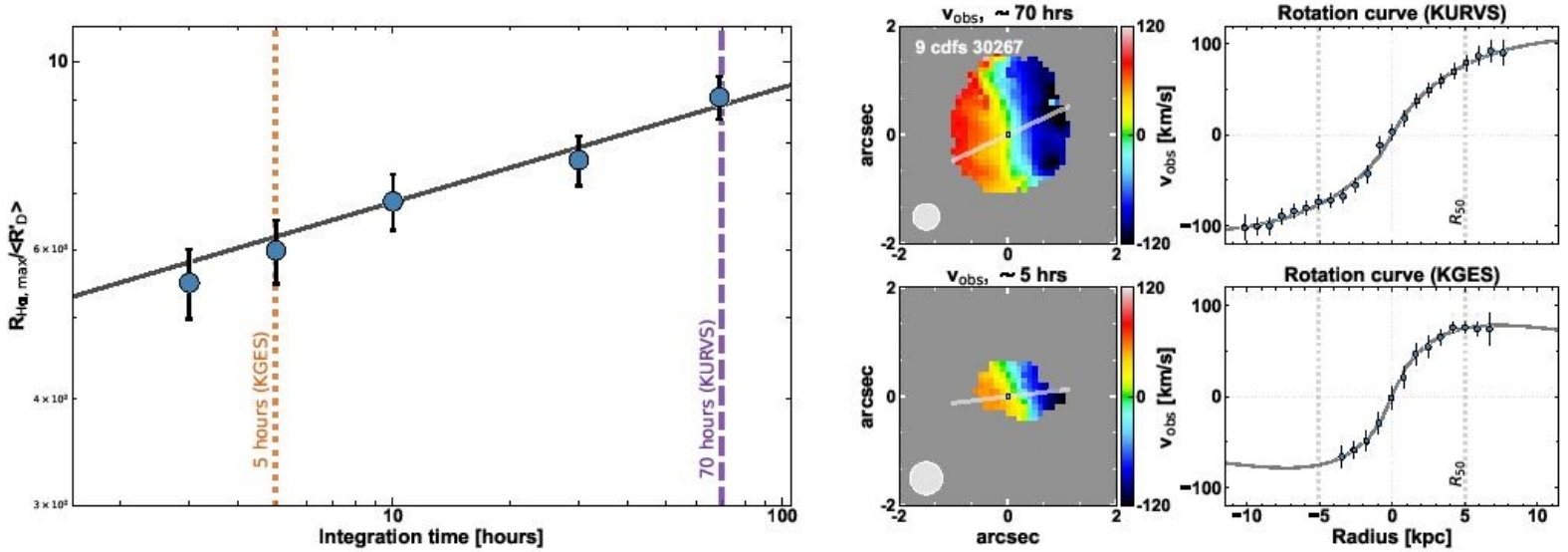

Figure 2. Left: Average radial extent of the Hα emission in KURVS galaxies as a function of integration time. Filled circles indicate the median extent of the Hα emission, derived as the square root of the area in which the Hα emission is detected with S/N$_{H\alpha} \geqslant 5$. The errorbars highlight the 1σ scatter of the distribution. Coloured vertical lines highlight the typical integration time of the parent sample from the KGES survey (dark orange) and KURVS (dark purple). For 70 hours of on-source integration, corresponding to the integration time in the KURVS survey, we robustly sample galaxy rotation curves out to $\sim R_{6D}$ for the average system. **Right:** Example of the velocity field and rotation curve from KURVS (top row) and KGES (bottom row) observations for the same galaxy. These are measured from KMOS data-cubes with a total on-source exposure time of ~70 and ~5 hours, respectively, as described in Section 3. The deep observations from KURVS allow us to measure high-quality velocity maps and rotation curves extending further out into the galaxy disc, as well as to derive the dynamical center with higher accuracy than pre-existent, shallower observations from KGES.

Еще примеры кинематики

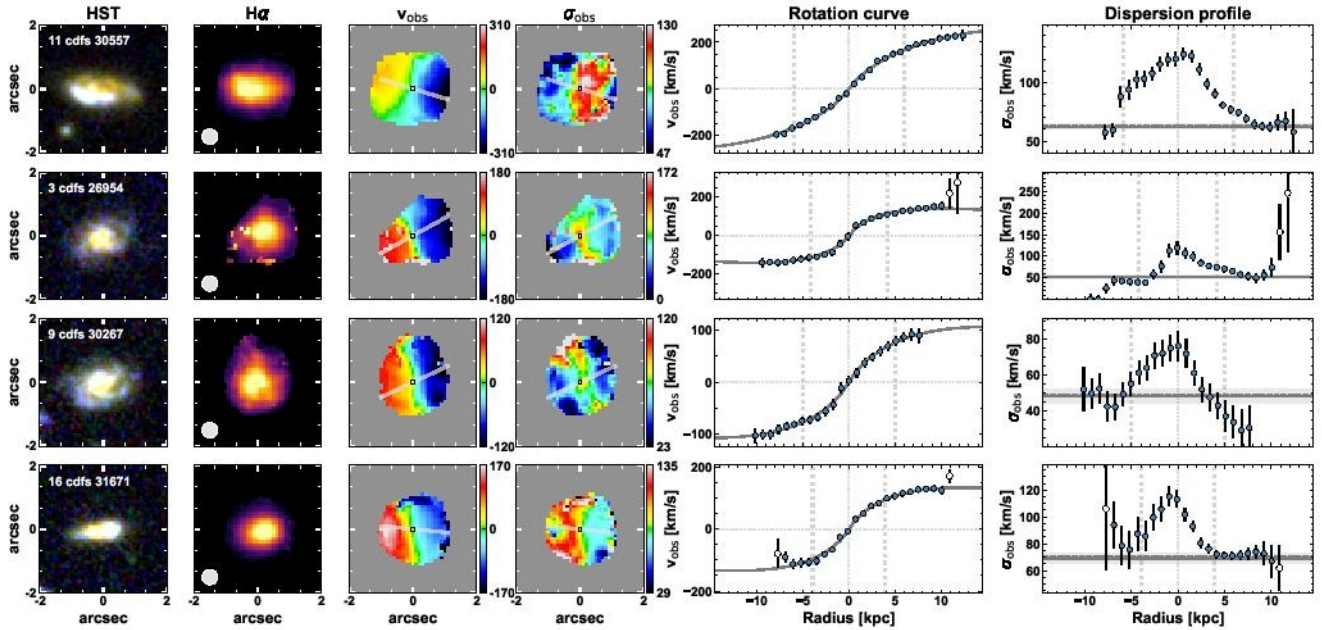

Figure 3. The KURVS data set. From left to right, the panels show the *HST* $B_{435} - z_{850} - H_{160}$ composite image, the Hα flux map, the line-of-sight velocity ($v_{\rm obs}$) and velocity dispersion ($\sigma_{\rm obs}$) maps, and the observed Hα rotation curve and velocity dispersion profile. These are extracted from the KURVS velocity and velocity dispersion maps along the kinematic major axis, indicated with a grey solid line in each map. Rotation curves are plotted such that the velocity gradient is always positive. Note that the colour scale in the velocity and velocity dispersion maps might differ from the range of velocities of the one-dimensional profiles since it is optimised to the range of velocities and velocity dispersions measured in two-dimensional data. The size of the PSF of KURVS observations is indicated by a grey filled circle in the bottom left of each Hα flux map. The white filled circles in the rotation curves and dispersion profiles indicate pixels that have been clipped due to either a large contamination from sky lines or broad components (see text for details). Here the thick dotted vertical lines mark the half-light radius measured from *HST* observations (R_{50}) for reference. The black solid curve in each rotation curve plot shows the best-fit exponential disc model to the data. For the dispersion profiles, the dotted grey and solid grey horizontal lines represent the observed and beam smearing corrected measure of the intrinsic dispersion, σ_0. The grey shaded area highlights the 1σ error of this quantity. The depth of KURVS observations allows us to probe the rotation curves of $z \sim 1.5$ star-forming galaxies out to ≥ 10 kpc, well beyond the stellar effective radius, hence providing important observational constraints on the amount of

Толстые диски, поддерживаемые вращением?

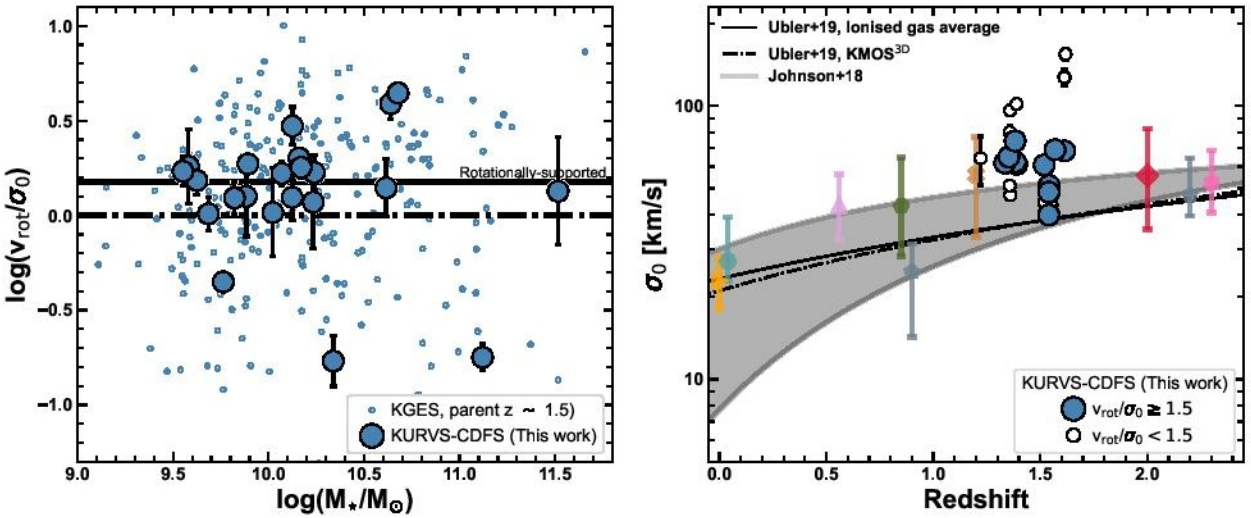

Figure 4. Left: Ratio between inclination corrected rotation velocity ($v_{\rm rot}$) and intrinsic velocity dispersion (σ_0) as a function of the stellar mass. The horizontal dash-dotted line marks the ratio $v_{\rm rot}/\sigma_0 = 1$, which has been used to distinguish "dispersion dominated" ($v_{\rm rot}/\sigma_0 < 1$) and "rotation dominated" ($v_{\rm rot}/\sigma_0 > 1$) galaxies in the literature (e.g., Wisnioski et al. 2015; Johnson et al. 2018). The horizontal solid line shows our conservative threshold $v_{\rm rot}/\sigma_0 = 1.5$ to identify rotationally-supported galaxies in KURVS. The fraction of rotationally-supported KURVS-CDFS galaxies is consistent with measurements of the discs fraction from KGES in a similar redshift and stellar mass range (Tiley et al. 2021). This is also consistent with KMOS^{3D} measurements when applying the same $v_{\rm rot}/\sigma_0 > 1$ cut (Wisnioski et al. 2019). **Right:** Intrinsic velocity dispersion (σ_0) as a function of redshift. Blue filled large circles and white small circles represent rotationally-supported and dispersion-dominated KURVS-CDFS galaxies, respectively. The coloured symbols are literature measurements for main-sequence star-forming galaxies at different redshifts (cyan circle: SAMI, Bryant et al. 2015; orange triangle: GHASP, Epinat et al. 2010; lilac triangle: MUSE, Swinbank et al. 2017; dark grey pentagons: KMOS^{3D}, Wisnioski et al. 2015, 2019; dark green hexagon: KROSS, Johnson et al. 2018; dark yellow cross: MASSIV, Epinat et al. 2012; red diamond: SIGMA, Simons et al. 2016; pink hexagon: SINS, Cresci et al. 2009). The solid line corresponds to the fit to literature measurements of the ionised gas velocity dispersion, and the dot-dashed line is the best-fit trend from KMOS^{3D} (Übler et al. 2019). The grey shaded area represent the redshift evolution of σ_0 for a Toomre disc instability toy model with $\log(M_\star/[\mathrm{M}_\odot]) = 9.8 - 10.8$ (Johnson et al. 2018), which corresponds to the $16^{\rm th} - 84^{\rm th}$ percentile range of the stellar mass distribution of the KURVS-CDFS sample (see Sect. 2.1). Rotationally-supported KURVS-CDFS galaxies follow the $\sigma_0 - z$ trend highlighted by previous studies. Overall, the integrated dynamical properties of KURVS-CDFS galaxies suggest that these are typical $z \sim 1.5$ star-forming discs at $\log(M_\star/[\mathrm{M}_\odot]) \sim 10.2$.

Все кривые вращения

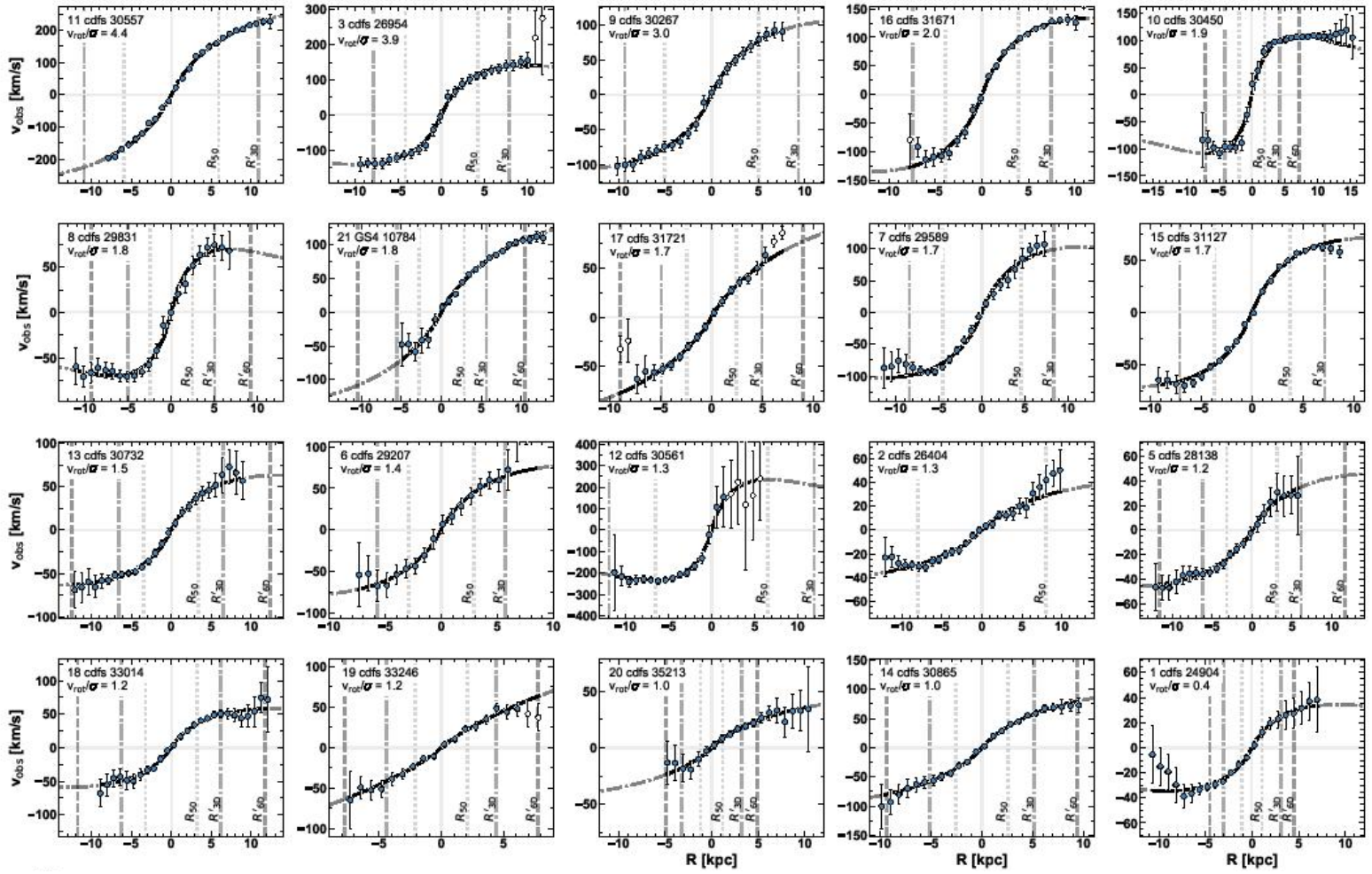

Результаты

Table 2. Kinematic properties of KURVS-CDFS galaxies.

KURVS ID	$R_{H\alpha,max}$ kpc	σ_0 km s^{-1}	v_{rot}/σ_0 km s^{-1}	t
(1)	(2)	(3)	(4)	(5)
1	10.7	96 ± 2	0.4 ± 0.1	1.05 ± 0.03
2	12.1	47 ± 1	1.3 ± 0.3	1.13 ± 0.12
3	11.7	51 ± 4	3.9 ± 0.1	0.92 ± 0.03
4	12.0	43 ± 2	0.2 ± 0.1	0.71 ± 0.05
5	12.1	44 ± 3	1.2 ± 0.2	1.19 ± 0.07
6	8.1	64 ± 13	1.4 ± 0.2	1.13 ± 0.10
7	11.4	61 ± 5	1.7 ± 0.2	0.98 ± 0.04
8	11.0	40 ± 3	1.8 ± 0.4	0.91 ± 0.03
9	10.2	48 ± 4	3.0 ± 0.3	1.04 ± 0.06
10⋆	15.2	61 ± 2	1.9 ± 0.1	0.99 ± 0.02
11	12.4	62 ± 2	4.4 ± 0.2	1.15 ± 0.04
12	11.2	127 ± 9	1.3 ± 0.3	0.67 ± 0.21
13	12.1	62 ± 4	1.5 ± 0.1	1.11 ± 0.05
14	9.8	102 ± 3	1.0 ± 0.1	1.28 ± 0.07
15	9.2	68 ± 4	1.7 ± 0.1	1.03 ± 0.03
16	10.9	69 ± 4	2.0 ± 0.1	1.02 ± 0.02
17	9.9	65 ± 3	1.7 ± 0.1	1.33 ± 0.12
18	12.1	61 ± 5	1.2 ± 0.1	1.11 ± 0.05
19	7.9	80 ± 4	1.2 ± 0.2	1.41 ± 0.38
20	10.4	51 ± 2	1.0 ± 0.3	1.18 ± 0.06
21	12.7	74 ± 2	1.8 ± 0.1	1.33 ± 0.08
22	13.6	155 ± 7	0.2 ± 0.1	0.65 ± 0.04

Table 3. Dark matter fraction of rotationally-supported KURVS-CDFS galaxies.

KURVS ID	$f_{DM}(\leqslant R_{eff})$
(1)	(2)
11	0.42 ± 0.09
13	0.62 ± 0.07
15	0.31 ± 0.13
16	0.50 ± 0.08
17	0.69 ± 0.06
21⋆	0.0
3	0.19 ± 0.13
7	0.46 ± 0.11
8	0.67 ± 0.06
9	0.54 ± 0.07

Note. (1) KURVS-ID. (2) Dark matter fraction within the effective radius and 1σ uncertainties. This is obtained on seeing- and pressure support-corrected rotation curves using equation 2. Galaxies are sorted in order of decreasing v_{rot}/σ_0. ⋆Galaxy KURVS-21 has a highly asymmetric velocity field, that makes it difficult to find a best-fitting model with GALPAK^{3D}. While we report its dark matter fraction for completeness, this measurements is highly unreliable and we flag this galaxy in the relevant plots.

Форма кривой вращения: сравнение с моделями

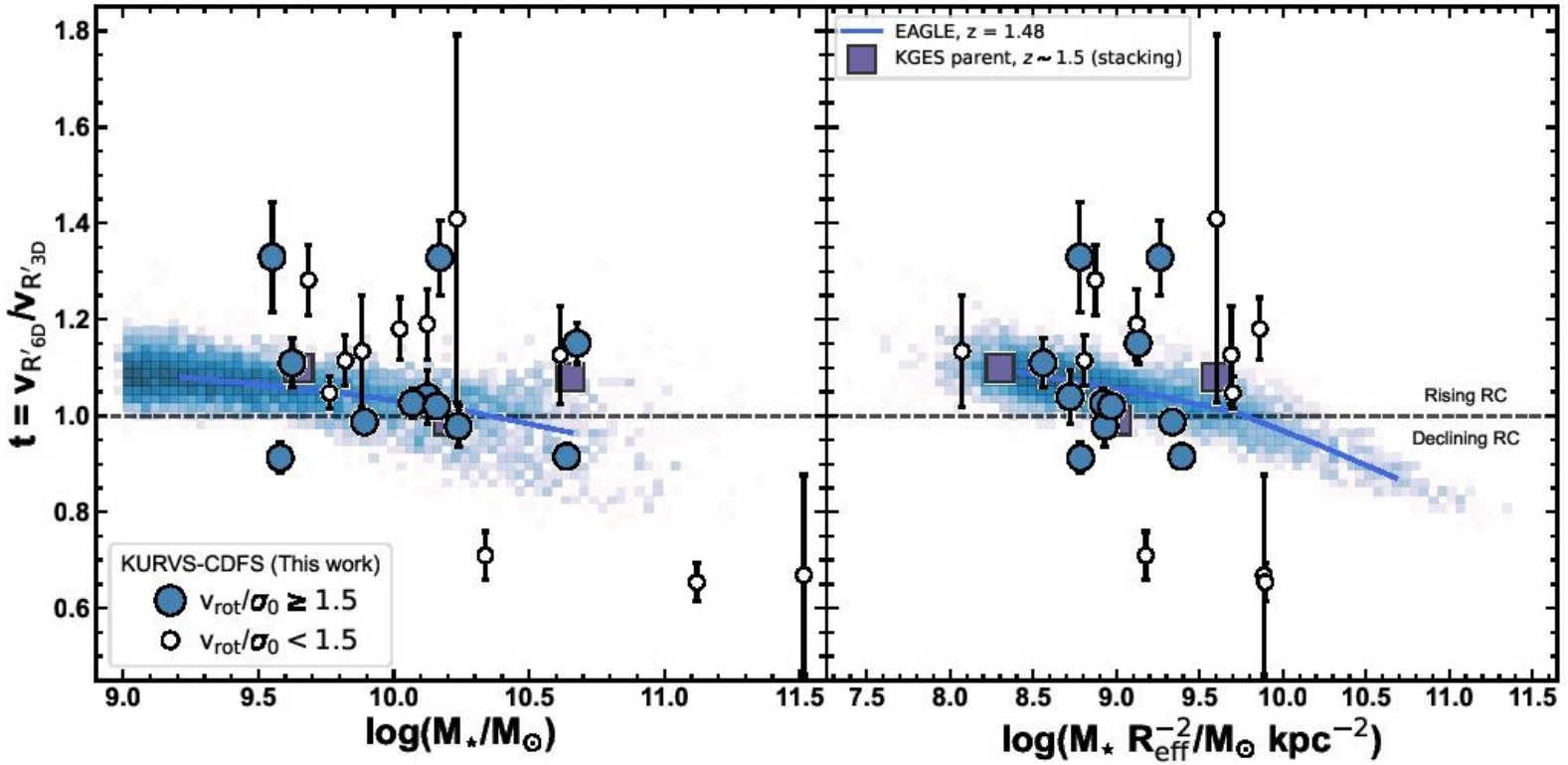

Figure 6. Outer rotation curve slope, $t = v_{R'_{6D}} / v_{R'_{3D}}$, as a function of stellar mass (left) and stellar mass surface density (right). Measurements for simulated EAGLE galaxies at $z = 1.48$ are displayed with a 2D density histogram in blue. The running median for EAGLE galaxies is shown as a blue solid line. Measurements from stacked rotation curves at $z \sim 1.5$ from the KGES survey are shown with purple squares for comparison with our previous work (Tiley et al. 2019b). Large filled blue circles and small white circles represent measurements for rotationally-supported and dispersion-dominated KURVS galaxies, respectively. The majority of observed rotation curves are flat or rising out to R'_{6D}, suggesting that $z \sim 1.5$ star-forming galaxies with stellar masses $\log(M_\star/M_\odot) \sim 10.2$ contain a large fraction of their total mass in the form of dark matter within this radius. Only three objects show substantially declining rotation curves. However, these have perturbed velocity fields and are dispersion-dominated. Therefore, measurements of the kinematics for such galaxies are highly uncertain. The observed rotation curve slopes are overall consistent with measurements of simulated EAGLE galaxies at similar redshifts.

Доля темной материи: сравнение с моделями

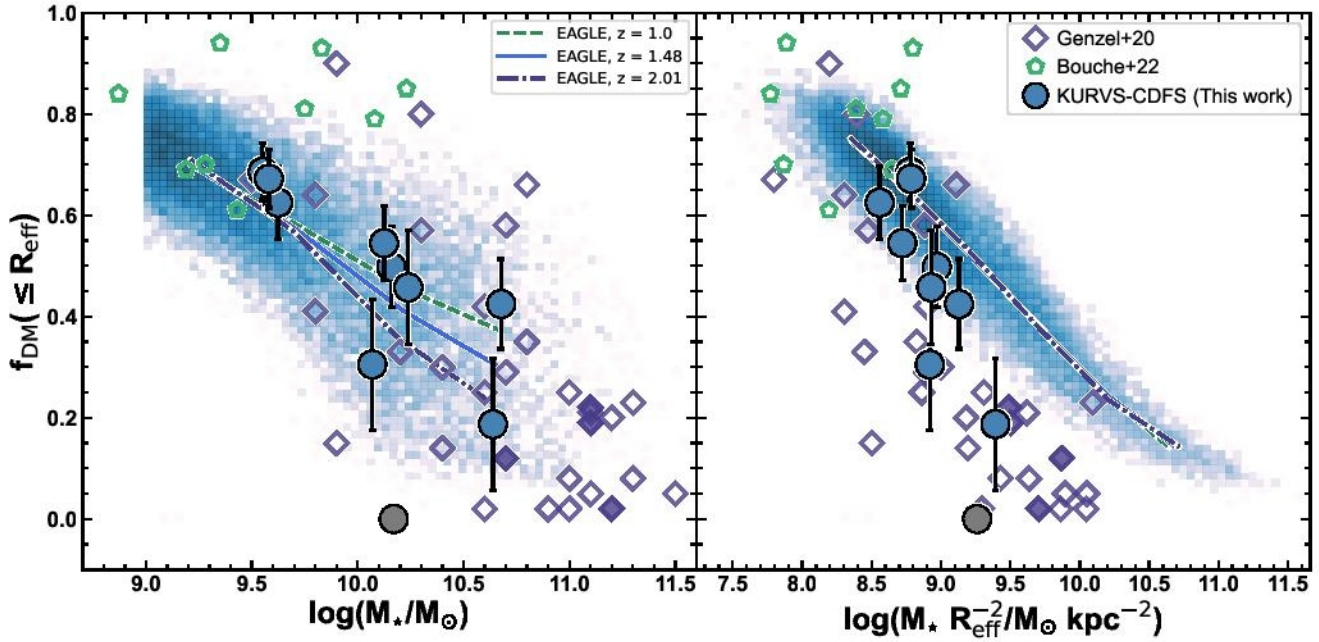

Figure 8. Dark matter fraction within the disc effective radius for high-redshift star-forming galaxies as a function of stellar mass (left) and stellar mass surface density (right). The 2D density histogram shows measurements for simulated EAGLE galaxies at $z = 1.0$, 1.48 and 2.01. The coloured lines show the running median at each redshift in EAGLE. The open green pentagons show the Bouché et al. (2022) sample of $z \sim 0.9$ star-forming galaxies. The open purple diamonds indicate the Genzel et al. (2020) sample at $0.67 \lesssim z \lesssim 2.45$, with filled symbols highlighting the sources that are in the same redshift range as our sample. Large filled circles represent rotationally-supported galaxies in KURVS-CDFS, with the grey data point indicating a source whose kinematics are not well-described by GALPAK^{3D}. Simulated EAGLE galaxies show a trend of decreasing dark matter fraction with increasing stellar mass, albeit with large scatter. Observed galaxies follow the same trend. There is a much tighter anti-correlation between the dark matter fraction and the stellar mass surface density in EAGLE. Observations follow a similar trend up to $\log(\Sigma_\star/M_\odot/\mathrm{kpc}^{-2}) \sim 9.2$. At higher stellar mass surface densities, however, EAGLE overpredicts the dark matter fraction of observed galaxies by a factor of ~ 3.

Еще сравнение с моделями

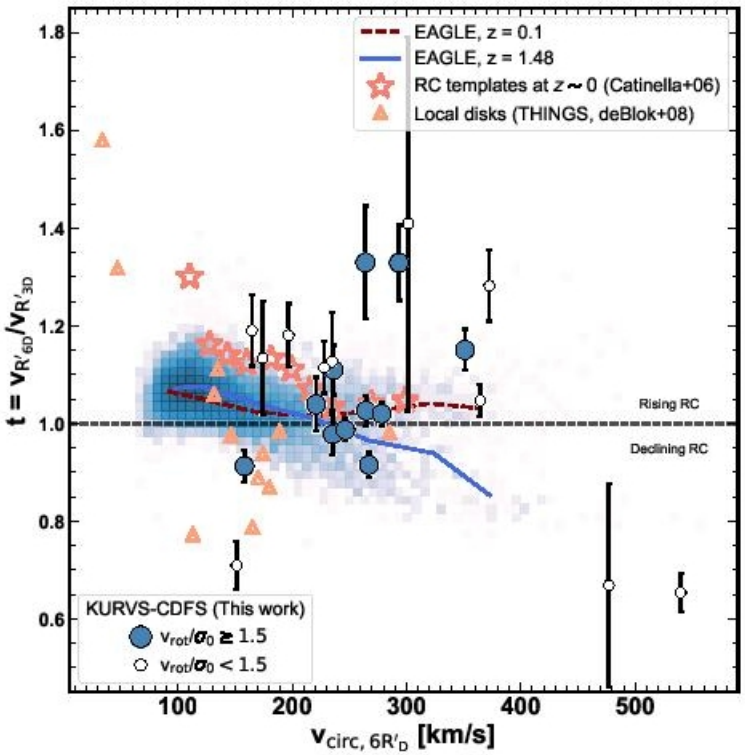

Figure 7. Outer rotation curve slope as a function of circular velocity at R_{6D} for local and high-redshift star-forming galaxies. The 2D density histogram shows measurements for simulated EAGLE galaxies at $z = 0.1$ and $z = 1.48$, with the coloured lines highlighting the running median at each redshift as specified in the legend. The colour code for KURVS-CDFS galaxies is analogous to Figure 6. Open light-orange triangles show measurements for local discs from the THINGS survey (De Blok et al. 2001; Trachternach et al. 2008), while the open pink stars indicate the rotation curve templates of local star-forming discs from Catinella et al. (2006). Outer rotation curve slopes of $z \sim 1.5$ star-forming galaxies are similar to measurements of local discs

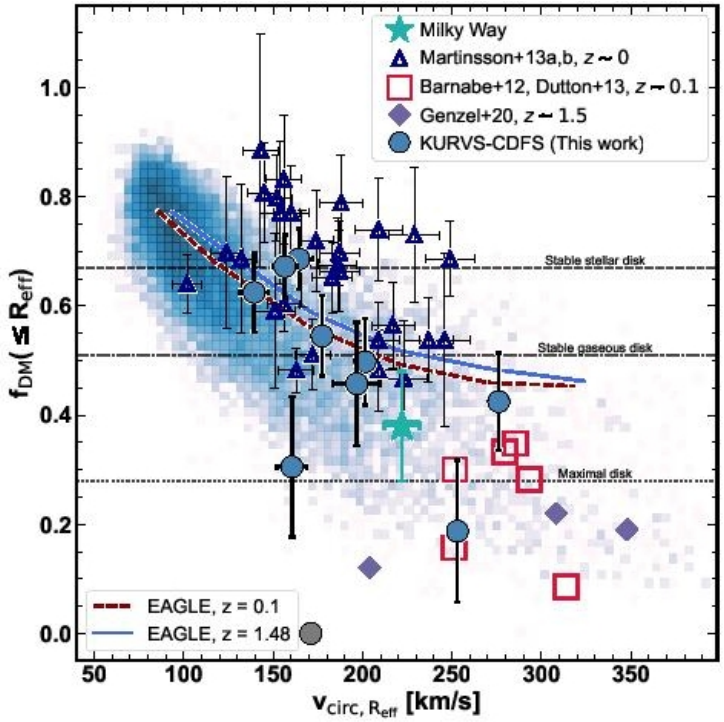

Figure 9. Dark matter fraction within the effective disc radius as a function of circular velocity at the effective radius for local and $z \sim 1.5$ star-forming galaxies. The 2D density histogram and coloured lines show measurements for simulated EAGLE galaxies at $z = 0.1$ and 1.48 as in Figure 7. The open dark blue triangles show measurements of $z \sim 0$ spirals from Martinsson et al. (2013a,b), and the filled green star indicate the dark matter fraction of the Milky Way (Bovy & Rix 2013; Bland-Hawthorn & Gerhard 2016). The open red squares indicate measurements of massive spiral galaxies with prominent bulges at $z \sim 0.1$ from the SWELLS survey (Barnabè et al. 2012; Dutton et al. 2013). The purple diamonds indicate the Genzel et al. (2020) galaxies in the redshift range of our survey. Large filled circles represent rotationally-supported galaxies in KURVS-CDFS, with the grey data point

ArXiv: 2305.02959

Evidence for Large Scale, Rapid Gas Inflows in z~2 Star Forming Disks

R. Genzel[1,2], J.-B. Jolly[1], D. Liu[1], S.H. Price[3], N.M. Förster Schreiber[1], L.J. Tacconi[1], R. Herrera-Camus[4], C. Barfety[1], A. Burkert[5], Y. Cao[1], R.I. Davies[1], A. Dekel[6], M.M. Lee[7,8], L.L. Lee[1], D. Lutz[1], T. Naab[9], R. Neri[10], A. Nestor Shachar[11], S. Pastras[1], C. Pulsoni[1], A. Renzini[12], K. Schuster[10], T.T. Shimizu[1], F. Stanley[10], A. Sternberg[1,11,13] & H. Übler[14,15]

[1]*Max-Planck-Institut für Extraterrestrische Physik (MPE), Giessenbachstraße 1, D-85748 Garching, Germany (genzel@mpe.mpg.de, forster@mpe.mpg.de, linda@mpe.mpg.de)*

[2]*Departments of Physics and Astronomy, University of California, Berkeley, CA 94720, USA*

[3]*Department of Physics and Astronomy and PITT PACC, University of Pittsburgh, Pittsburgh, PA 15260, USA*

[4]*Astronomy Department, Universidad de Concepción, Av. Esteban Iturra s/n Barrio Universitario, Casilla 160, Concepción, Chile*

[5]*Universitäts-Sternwarte Ludwig-Maximilians-Universität (USM), Scheinerstraße 1, D-81679 München, Germany*

[6]*Racah Institute of Physics, The Hebrew University of Jerusalem, Jerusalem 9190401, Israel*

[7]*Cosmic Dawn Center (DAWN), Denmark*

[8]*DTU-Space, Technical University of Denmark, Elektrovej 327, DK2800 Kgs. Lyngby, Denmark*

[9]*Max-Planck Institute for Astrophysics, Karl-Schwarzschild-Straße 1, D-85748 Garching, Germany*

[10]*Institut de Radioastronomie Millimétrique (IRAM), 300 rue de la Piscine, F-38406, Saint Martin d'Hères, France*

[11]*School of Physics and Astronomy, Tel Aviv University, Tel Aviv 69978, Israel*

[12]*Osservatorio Astronomico di Padova, Vicolo dell'Osservatorio 5, Padova, I-35122, Italy*

[13]*Center for Computational Astrophysics, Flatiron Institute, 162 5th Avenue, New York, NY 10010, USA*

[14]*Kavli Institute for Cosmology, University of Cambridge, Madingley Road, Cambridge, CB3 0HA, UK*

[15]*Cavendish Laboratory, University of Cambridge, 19 JJ Thomson Avenue, Cambridge, CB3 0HE, UK*

9 галактик: KMOS+CO

Table 1. Basic Properties of the Galaxies

source	z	R_e	$v_c(R_e)$	σ_0	v_c/σ_0	$\log M_{baryon}$	B/T	SFR	$f_{DM}(R_e)$	f_{gas}	$\sin i$	Q	t_{int}
…	…	(kpc)	(km s^{-1})	(km s^{-1})	…	($M_\odot$)	…	($M_\odot$yr^{-1})	…	…	…	…	(hr)
(1)	(2)	(3)	(4)	(5)	(6)	(7)	(8)	(9)	(10)	(11)	(12)	(13)	(14)
EGS_13035123	1.12	10.2	220	19	11.6	11.04	0.20	126	0.3	0.40	0.41	0.27	61
zC_403741	1.45	2.6	206	60	3.4	10.59	0.70	60	0.1	0.38	0.47	1.00	12
GS4_43501	1.61	4.9	259	60	4.3	10.92	0.05	53	0.3	0.45	0.88	0.58	22
Q2343_BX610	2.21	4.0	295	60	4.9	10.94	0.12	140	0.3	0.62	0.63	0.47	58
K20_ID7	2.23	7.9	322	60	5.4	11.27	0.04	101	0.6	0.64	0.85	0.37	33
Q2346_BX482	2.26	5.8	293	67	4.4	10.91	0.02	80	0.6	0.63	0.87	0.52	18
zC_405226	2.29	5.9	120	54	2.2	10.30	0.63	117	0.6	0.75	0.81	0.71	15
D3a_15504	2.38	6.1	266	68	3.9	11.18	0.30	146	0.2	0.43	0.64	0.68	47
D3a_6004	2.39	4.9	432	60	7.2	11.43	0.49	355	0.1	0.37	0.42	0.58	23

Notes: Columns (1) to (13) are updated galaxy properties for our galaxies selected from the RC100 sample (Nestor et al. 2023): source name radius (R_e), circular velocity at R_e ($v_c(R_e)$), intrinsic velocity dispersion (σ_0), circular velocity to velocity dispersion ratio (v_c/σ_0), baryon m ratio, star formation rate, dark matter fraction within R_e, gas fraction (f_{gas}), sine of inclination angle ($\sin i$), and Toomre Q parameter. Al consistent with RC100 (Nestor et al. 2023, Table B1) to within the 1σ uncertainty, except that for BX610 we updated SFR from far-infrared-b Brisbin et al. 2019). Columns (14) and (15) are the on-source integration time and FWHM of the angular resolution of the IFU data used in thi

После построения и вычитания модели кругового вращения – искали радиальные движения

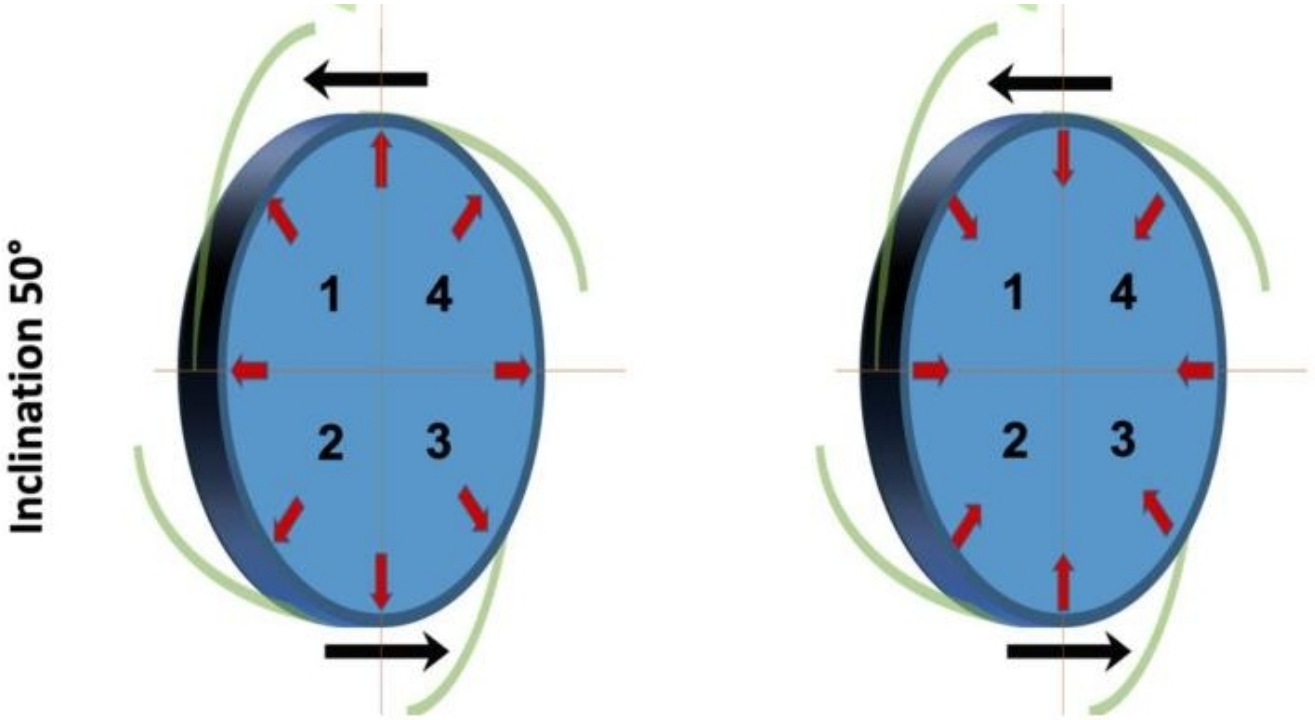

Пример (хотя и нетипичный)

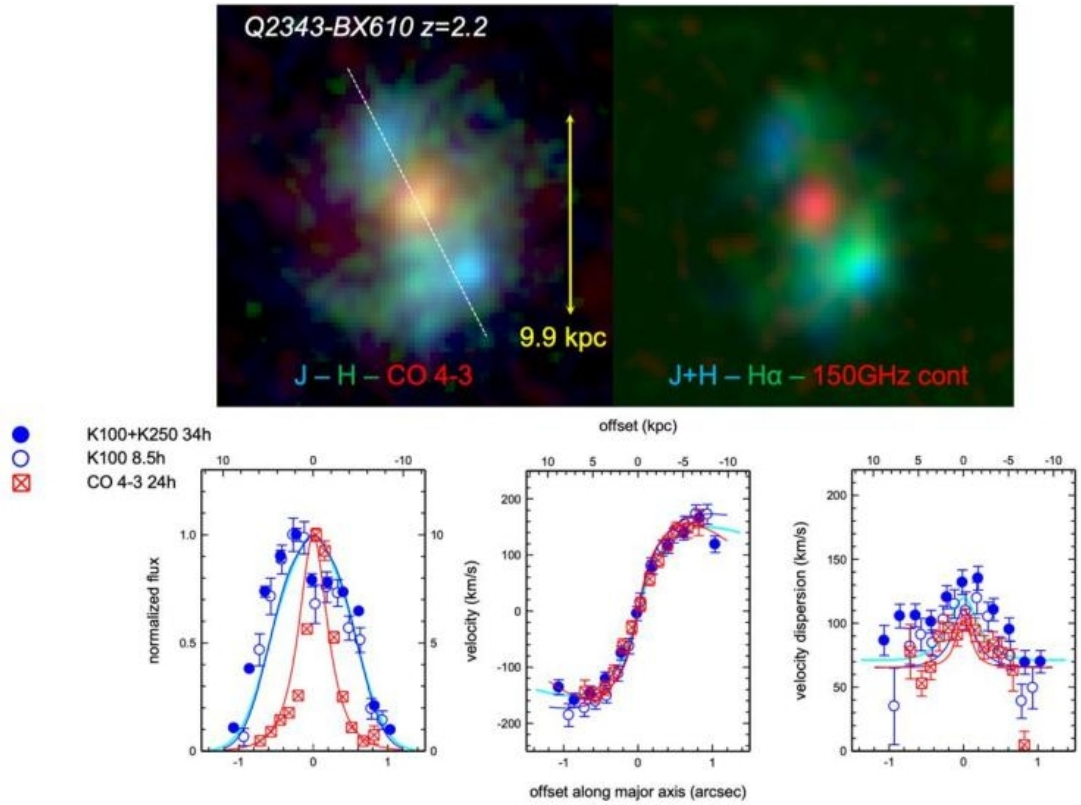

Figure 4. Top left: Combined HST J-H continuum (blue and green), and integrated ALMA CO 4-3 (red), all at ~0.2″ FWHM resolution. The dotted white line marks the direction of the bar-like structure. Top right: Combined HST J+H continuum (blue), and integrated ALMA rest 460 GHz continuum (red), and Hα integrated line (green), at ~0.25–0.3″ FWHM resolution. Bottom: 1^D cuts along the major axis at $PA_{major} \sim -20$ to $-30°$ in CO 4-3 (red squares), Hα AO (open blue circles) and Hα AO + non-AO (filled blue circles) in line intensity (left), line velocity (center) and line velocity dispersion (right).

Ее поля скоростей

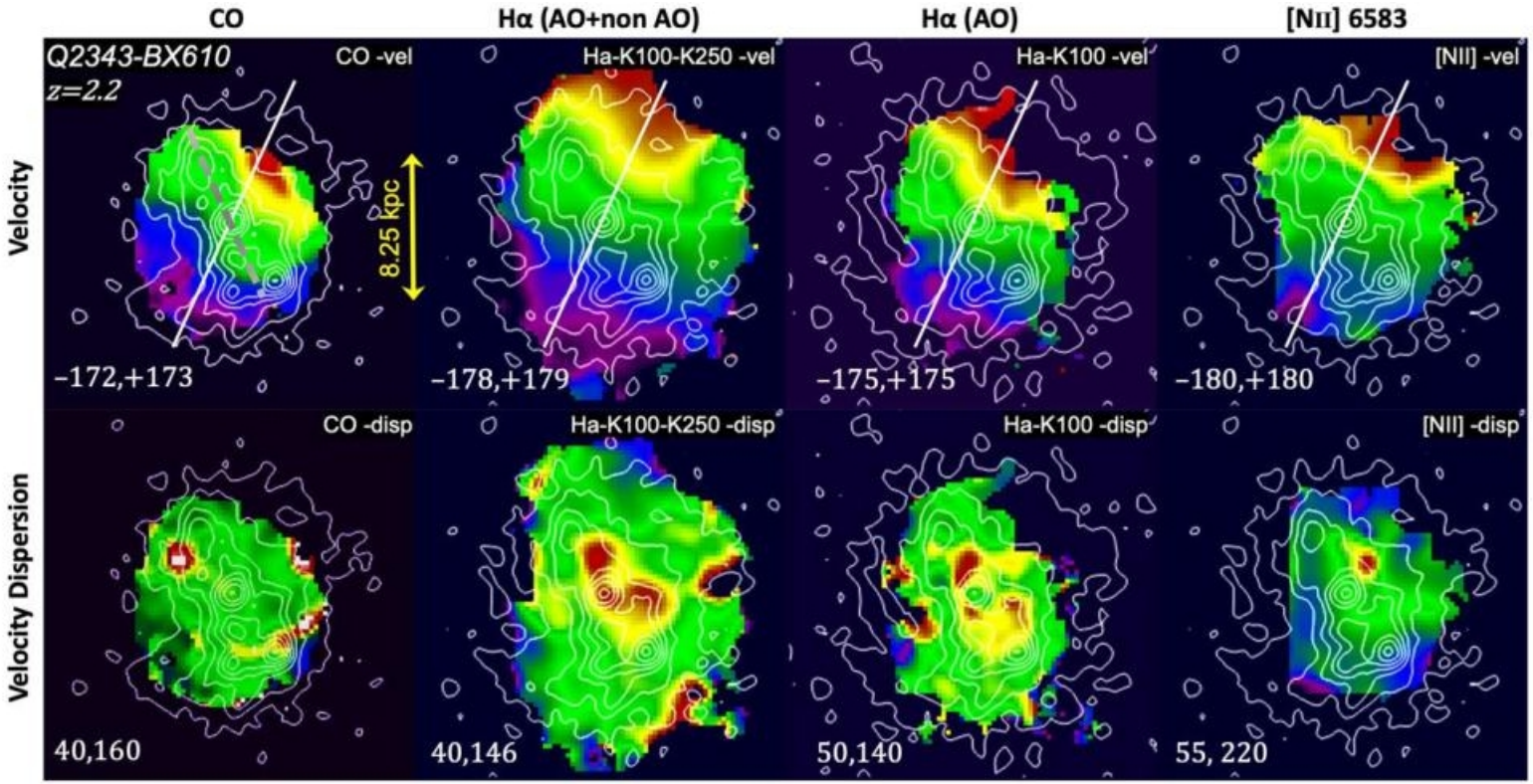

Figure 5. Velocity (top) and velocity dispersion (bottom) maps in CO 4-3 (left), Hα non AO+AO (second from left), Hα AO (third from left) and [NII] 6583 (right), superposed on the HST H-band map in contours. The color indicates the velocity amplitude with the numbers at the bottom of each panel giving the mininum (purple) and maximum (red) values. The yellow arrow denotes 1". The kinematic major axis of the galaxy at $PA_{major} \sim -25 \pm 5°$ *is marked as a white line, and the zero iso-velocity contour ridge (green color) at* $PA \sim 24°$ *is indicated by the gray dashed line in the first panel.*

Ее поля ОСТАТОЧНЫХ скоростей

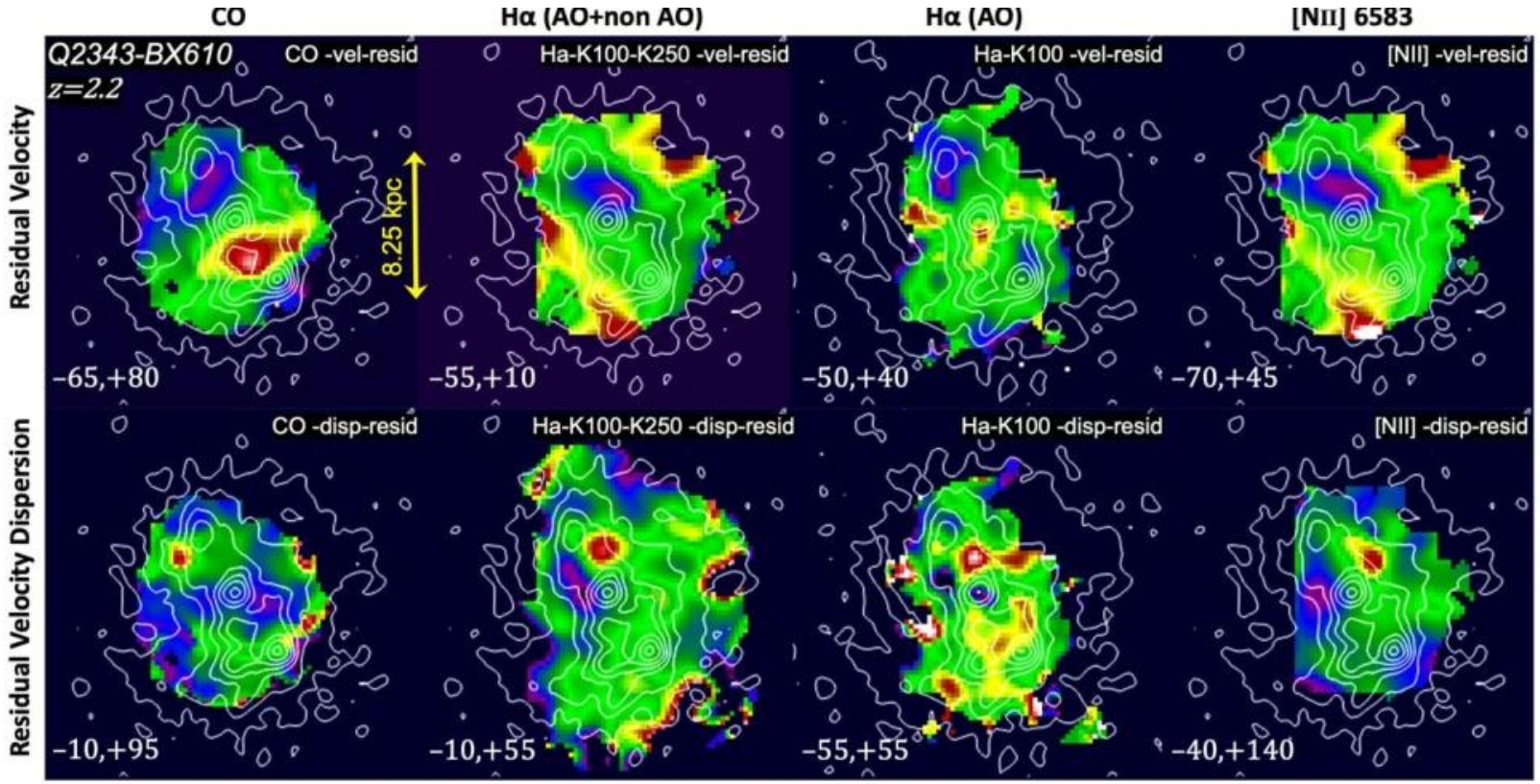

Figure 6. Velocity residual (top) and velocity dispersion residual (bottom) maps of the CO 4-3 (left), Hα AO+ non AO second from left), Hα AO (third from left) and [NII] 6583 AO + non AO data (right), after subtracting the corresponding ***DYSMAL*** *model maps from our data. Color scheme and amplitudes are the same as in Figure 5.*

Результаты для всех

Table 2. Fitting Results for inflow velocities and kinemetry

Source	z	v_{resid} (km s^{-1})	δv_{resid} (km s^{-1})	$v_{resid,SP}$ (km s^{-1})	$v_{resid,DL}$ (km s^{-1})	$v_r(obs) = v_{resid}/\sin i$ (km s^{-1})	$\delta v_r(obs)$ (km s^{-1})	$v_r(Toomre)$ (km s^{-1})	$\delta v_r(Toomre)$ (km s^{-1})	$\frac{v_r(obs)}{v_r(Toomre)}$	$\delta\frac{v_r(obs)}{v_r(Toomre)}$	$\frac{v_r}{v_c}$
(1)	(2)	(3)	(4)	(5)	(6)	(7)	(8)	(9)	(10)	(11)	(12)	(13)
EGS_13035123	1.12	17	7	…	17	42	14	31	8	1.37	0.57	0.19
zC_403741	1.45	20	10	…	…	43	21	26	6	1.65	0.92	0.21
GS4_43501	1.61	27	12	…	25	31	14	46	11	0.70	0.30	0.12
Q2343_BX610	2.21	60	15	50	70	95	24	98	25	0.97	0.34	0.32
K20_ID7	2.23	75	15	85	55	87	17	114	29	0.76	0.24	0.27
Q2346_BX482	2.26	65	25	55	60	75	29	101	25	0.74	0.34	0.26
zC_405226	2.29	82	30	…	…	101	37	59	15	1.73	0.77	0.84
D3a_15504	2.38	50	25	60	55	78	39	43	11	1.82	1.02	0.29
D3a_6004	2.39	50	20	80	55	118	47	51	13	2.31	1.09	0.27

Результаты для всех

Source	z	$PA_{major,light}$	$PA_{major,kin}$	PA_{resid}	δPA	rotational motion on sky	i	radial motions	shape of outer rotation curve
…	…	(deg)	(deg)	(deg)	(deg)	…	(deg)	…	…
(1)	(2)	(3)	(4)	(5)	(6)	(7)	(8)	(9)	(10)
EGS_13035123	1.12	-175	-167	-70	97	clockwise	156	inflow along/near minor axis	peak-drop
zC_403741	1.45	-149	-143	-48	95	clockwise?	152	inflow along/near minor axis?	peak-drop
GS4_43501	1.61	-32	-32	75	107	clockwise	118	inflow along/near minor axis	dropping
Q2343_BX610	2.21	-25 ± 5	-25 ± 5	-156 ± 5	-131	counter-clockwise	39	inflow along the bar at $PA \sim 25°$, 40° off minor axis	peak
K20_ID7	2.23	-164	-156	-54	102	clockwise	122	inflow along/near minor axis	rising
Q2346_BX482	2.26	121	111	-39	-150	counter-clockwise	60	inflow along axis different than minor axis	rising
zC_405226	2.29	116	150	240	90	clockwise	126	inflow along/near minor axis	flat
D3a_15504	2.38	164	155	67	-88	counter-clockwise?	40	inflow along/near minor axis, but if clockwise out-flow	dropping
D3a_6004	2.39	37	167	52	-115	counter-clockwise	25	inflow near minor axis	peak

Рост скорости втекания с z объясняют увеличением массы газа (по Тумре)

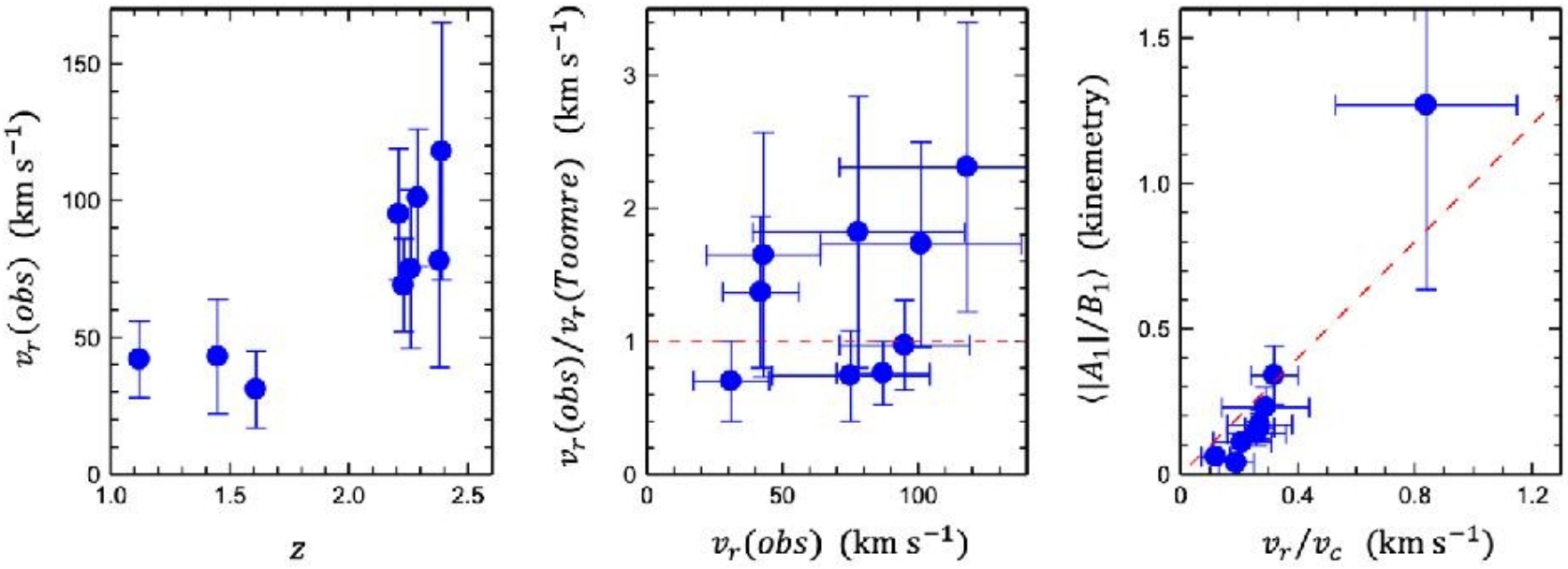

Figure 8. Correlation between derived properties of the nine galaxies. For the computation of the theoretically expected converging flow speed (Table 2) we use equation 11 with a~1.75, ζ=2 and γ=0. We also use for each galaxy the estimates of gas fraction and Q as given in Table 1.